Journal of Solid State Chemistry **147,** 259–268 (1999)
Article ID jssc.1999.8253, available online at http://www.idealibrary.com on IDEAL®

Structural Investigation and Luminescence Properties of the $Ce_3(SiS_4)_2X$ (X = Cl, Br, I) Family and the $La_{3-x}Ce_x(SiS_4)_2I$ ($0 \leq x \leq 1$) Solid Solution

Regis Riccardi,* Delphine Gout,* Gilles Gauthier,* François Guillen,† Stéphane Jobic,* Alain Garcia,† Denis Huguenin,‡ Pierre Macaudière,‡ Claude Fouassier,†,[1] and Raymond Brec*,[1]

*Institut des Matériaux de Nantes, BP 32229, 44322 Nantes Cedex 03, France; †Institut de Chimie de la Matière Condensée de Bordeaux, CNRS, Avenue du Dr. A. Schweitzer, 33608 Pessac Cedex, France; and ‡Centre de Recherches de Rhodia, 52 rue de la Haie Coq, 93308 Aubervilliers Cedex, France

Received December 7, 1998; in revised form February 19, 1999; accepted February 24, 1999

Recently prepared $Ce_3(SiS_4)_2I$ exhibits a strong room temperature luminescence in the blue region of the visible spectrum associated to a Ce^{III}-$5d^1 \rightarrow Ce^{III}$-$4f^1$ electronic transition. In order to approach the emission mechanisms, the $La_{3-x}Ce_x(SiS_4)_2I$ family has been investigated by optical techniques at 6 and 300 K. At low temperature luminescence of the two crystallographically distinct cerium cations was evidenced along with an intrinsic luminescence of the lanthanum matrix. The influence of the halogenide on the optical properties has been studied through the substitution of iodine by chlorine and bromine which permits us to follow the increase in energy of the 4*f*–5*d* gap in the Cl < Br < I series. © 1999 Academic Press

1. INTRODUCTION

Recently, the synthesis, structure, and electronic properties of the first cerium iodothiosilicate $Ce_3(SiS_4)_2I$ was reported (1, 2). At this occasion, it was pointed out that the pale yellow coloration of the material was associated to the promotion of an Ce^{III}-4*f* electron to the Ce^{III}-5*d* band. On the course of the optical characterization of this compound, a room temperature strong luminescence in the blue part of the visible spectrum was observed under UV excitation.

In rare earth halooxosilicates, cerium has already shown the ability to give an emission in the near ultraviolet (3–5). In their sulfide analogues, the luminescence band lies in the visible range, owing to the higher covalency of the Ce–S bond. This explains why cerium-activated sulfides are of great interest for use as blue phosphors in electroluminescent devices. For such an application, the highest efficiencies have been obtained with SrS:Ce, even though in this case a large part of the blue-green emission must be eliminated by filtering, so as to obtain a color suitable for display (6). This problem has been partly solved in the $SrGa_2S_4$:Ce compound, which yields a blue emission that does not require any filtering (7).

After a crystal structure investigation of the $Ln_3(SiS_4)_2X$ (Ln = La, Ce; X = Cl, Br, I) family, an optical study is presented whose aim was to analyze:

(1) the influence of the Ce–X bonding in the $Ce_3(SiS_4)_2X$ (X = Cl, Br, I) series on the absorption and emission due to Ce^{III},

(2) the intrinsic luminescence of Ce^{III} in the absence of concentration quenching in some ($La_{3-x}Ce_x(SiS_4)_2I$ with $0 < x < 1$) solid solutions.

2. EXPERIMENTAL

2.1. Synthesis

The $Ce_3(SiS_4)_2X$ (X = Cl, Br, I) compounds were prepared from silicon (Cerac, − 325 mesh, 99.99%), sulfur (Fluka, puriss. > 99.999%), and Ce_2S_3 (Cerac, − 325 mesh, 99.9%). The halogen sources were from $CeCl_3$ (Cerac, 99.9%), $CeBr_3$ (Cerac, 99.9%), and iodine (Alfa, 99.9%). In each case, the reactants were taken in the ratio Ce:Si:X:S = 3:3:1:10, ($Ce_3(SiS_4)_2X$:SiS_2 = 1:1), i.e., with an excess of silicon sulfide. The reactants were handled in a dry box under nitrogen atmosphere, weighted in the aforementioned ratios, and placed in silica tubes. These latter were evacuated (10^{-3} torr) after cooling in liquid nitrogen and flame sealed. Each sample was heated at 300°C for 2 days and then at 900°C for 7 days. The samples were then slowly cooled to room temperature. The SiS_2 excess was found to be condensed at the colder end of the reaction tube, leaving a well-crystallized $Ce_3(SiS_4)_2X$ powder at the warmer end. The color of these powders, greenish white, bluish white and beige for X = Cl, Br, and I, respectively, is caused by the lower energy 4*f* → 5*d* transition of cerium and influenced by the presence of defects (see below).

[1]To whom correspondence should be addressed.

0022-4596/99 $30.00

$La_3(SiS_4)_2I$ and the $La_{3-x}Ce_x(SiS_4)_2I$ solid solution phases ($x = 0.01$, 0.03, 0.1, 0.2, 0.5, 0.8, and 1) were prepared from SiS_2 (Cerac, 99.5%), iodine (Alfa, 99.9%), La_2S_3 (Cerac, -325 mesh powder, 99.9%), and Ce_2S_3 (Cerac, -325 mesh powder, 99.9%). Once the reactants were intimately ground, the same handling and sealing procedures as above were used for the corresponding molar ratios La:Ce:Si:I:S = $3-x$:x:3:1:10.5, i.e., $La_{3-x}Ce_x(SiS_4)_2I:SiS_2:S = 1:1:0.5$. A higher crystalline quality was obtained for the solid solution and $La_3(SiS_4)_2I$ by using the following slightly modified heating procedure: the samples were heated at 400°C for 1 day, then at 850°C for 7 days, and slowly cooled to room temperature afterward. Again, the SiS_2 excess separated easily from the solid solution within the reaction tube.

2.2. Structural Characterization

The $Ln_3(SiS_4)_2X$ (Ln = Ce, La, X = Cl, Br, I) phases were examined by X-ray powder diffraction. Each powder was sieved at 50 μm and introduced, under dry nitrogen, in a Lindemann capillary (diam. 0.1 mm). The diagrams were recorded at room temperature with an INEL diffractometer using a monochromatized radiation CuK-L_2 (λ = 1.540598 Å), equipped with a CPS120 detector calibrated with $Na_2Ca_3Al_{12}F_{14}$ as standard (8) and set up in a Debye–Scherrer geometry. The data were first analyzed by the Prolix and the U-fit programs (9). All compounds turn to be isostructural to $Ce_3(SiS_4)_2I$ (1, 2). In each case, the diagram reflections (hkl) assignment and ensuing cell parameters refinement left no lines unaccounted for, indicating (i) a good purity of the sample at the X-ray diffraction detection threshold and (ii) a random La/Ce distribution in the $La_{3-x}Ce_x(SiS_4)_2I$ ($0 \le x \le 1$) solid solutions.

After a full pattern matching analysis (Fullprof (10)) of the corresponding data file (2θ range: 10°–110°, $\Delta 2\theta$ step: 0.03°, number of reflections ~850) including a pseudo-Voigt and Cagliotti description of the peak shapes and halfwidths with two parameters of low theta asymmetry, the structure refinements of the X-ray powder diagrams by the Rietveld method were performed in the $C2/c$ (No. 15) space group of the monoclinic symmetry ($Z = 4$) with the software Fullprof (10). Absorption corrections were made using the linear absorption coefficient formula (11), the sample thickness r (radius of the capillary) being corrected by a powder compacity factor of 0.35. Even with these precautions, some difficulties arose in the refinement of the sulfur isotropic atomic displacement parameters (ADP_{iso}), probably due to the strong absorption of cerium. The sulfur ADP_{iso} had to be set equal to one another. Under these conditions, the refinements could be carried out satisfactorily. The conditions and results of the refinement of the chloride and bromide compounds, $Ce_3(SiS_4)_2Cl$ and $Ce_3(SiS_4)_2Br$, and of three iodide derivatives ($La_3(SiS_4)_2I$, $La_2Ce(SiS_4)_2I$, and $Ce_3(SiS_4)_2I$) are summarized in Table 1. The atomic fractional coordinates and the ADP_{iso} are given in Table 2, except those of the already published $Ce_3(SiS_4)_2I$ phase (1,2). Selected bond distances and angles in the $Ce_3(SiS_4)_2X$ (X = Cl, Br) series can be found in Table 3, those for $Ce_3(SiS_4)_2I$ are listed in (2). Lists of refinement parameters and atomic positions of the $La_{3-x}Ce_x(SiS_4)_2I$ ($x = 0.01$, 0.03, 0.1, 0.2, 0.5, and 0.8) solid solutions are available on request.

TABLE 1
Results of the Structural Refinement (Rietveld Method) for $Ce_3(SiS_4)_2Cl$, $Ce_3(SiS_4)_2Br$, $La_3(SiS_4)_2I$, $La_2Ce(SiS_4)_2I$, and $Ce_3(SiS_4)_2I$

	$Ce_3(SiS_4)_2Cl$	$Ce_3(SiS_4)_2Br$	$La_3(SiS_4)_2I$	$La_2Ce(SiS_4)_2I$	$Ce_3(SiS_4)_2I$
Cos(θ)-shift parameter	0.016(2)	0.001(2)	0.060(1)	−0.048(4)	0.002(2)
Overall scale factor	0.000497(3)	0.000527(4)	0.000269(1)	0.000105(1)	0.000670(5)
Cell parameters	a = 15.6187(6) Å b = 7.7103(3) Å c = 10.9841(3) Å β = 96.970(2)° V = 1312.99(9) Å^3	a = 15.7150(4) Å b = 7.7643(2) Å c = 10.9344(3) Å β = 97.295(1)° V = 1323.37(6) Å^3	a = 16.0920(3) Å b = 7.9117(1) Å c = 10.9296(2) Å β = 97.959(1)° V = 1378.10(5) Å^3	a = 16.057(1) Å b = 7.8916(6) Å c = 10.9116(8) Å β = 97.939(4)° V = 1369.4(2) Å^3	a = 15.9735(5) Å b = 7.8559(2) Å c = 10.8734(3) Å β = 97.935(2)° V = 1351.40(7) Å^3
η (pseudo-Voigt)	0.50(2)	0.33(2)	0.33(1)	0.14(4)	0.28(2)
Halfwidth parameters (Cagliotti)	U = 0.077(8) V = −0.035(6) W = 0.026(1)	U = 0.023(2) V = −0.018(2) W = 0.0142(5)	U = 0.044(2) V = −0.039(2) W = 0.0201(5)	U = 0.14(2) V = −0.10(1) W = 0.041(2)	U = 0.039(4) V = −0.036(4) W = 0.0211(8)
Asymmetry parameters ($2\theta < 40°$)	0.110(6),0.019(2)	0.00(1),0.007(2)	0.108(7),0.041(2)	0.05(2),0.049(5)	0.117(9),0.045(3)
Reliability factors	R_p = 2.38, R_{wp} = 3.02 R_{exp} = 1.69, χ^2 = 3.19	R_p = 2.26, R_{wp} = 2.97 R_{exp} = 1.42, χ^2 = 4.35	R_p = 1.72, R_{wp} = 2.32 R_{exp} = 2.95, χ^2 = 0.619	R_p = 1.96, R_{wp} = 2.51 R_{exp} = 2.20, χ^2 = 1.31	R_p = 4.60, R_{wp} = 5.98 R_{exp} = 2.72, χ^2 = 4.85

TABLE 2

Fractional Atomic Coordinates and Isotropic Atomic Displacement Parameters of $Ce_3(SiS_4)_2X$ ((a) X = Cl, (b) X = Br), (c) $La_3(SiS_4)_2I$ and (d) $La_2Ce(SiS_4)_2I$

Atom	x	y	z	ADP_{iso} (Å^2)
		(a)		
Ce(1)	0.1920(2)	0.1188(4)	0.6852(2)	1.05(8)
Ce(2)	1/2	0.1185(6)	3/4	0.9(1)
Cl	0	0.001(2)	1/4	2.0(5)
Si	0.1590(8)	0.462(2)	0.026(1)	0.3(3)
S(1)	0.1434(7)	0.254(1)	0.133(1)	0.9(1)
S(2)	0.2883(7)	0.572(1)	0.086(1)	0.9
S(3)	0.0629(7)	0.667(1)	0.049(1)	0.9
S(4)	0.1494(7)	0.412(1)	− 0.1584(9)	0.9
		(b)		
Ce(1)	0.1939(2)	0.1193(4)	0.6835(2)	0.80(6)
Ce(2)	1/2	0.1084(6)	3/4	1.2(1)
Br	0	0.9891(9)	1/4	2.2(2)
Si	0.1580(9)	0.471(2)	0.026(1)	1.3(3)
S(1)	0.1442(7)	0.254(1)	0.141(1)	0.6(1)
S(2)	0.2837(7)	0.573(1)	0.0857(9)	0.6
S(3)	0.0674(6)	0.655(1)	0.0468(9)	0.6
S(4)	0.1494(6)	0.404(1)	− 0.1559(8)	0.6
		(c)		
La(1)	0.1962(1)	0.1200(3)	0.6801(2)	0.67(5)
La(2)	1/2	0.0941(4)	3/4	0.61(8)
I	0	0.9857(4)	1/4	1.68(9)
Si	0.1579(7)	0.459(1)	0.0293(9)	1.1(3)
S(1)	0.1449(5)	0.2577(9)	0.1434(7)	0.38(9)
S(2)	0.2786(5)	0.567(1)	0.0838(7)	0.38
S(3)	0.0671(5)	0.6491(9)	0.0424(7)	0.38
S(4)	0.1525(5)	0.404(1)	− 0.1557(7)	0.38
		(d)		
Ce(1)/La(1)	0.1975(3)	0.1186(7)	0.6805(5)	1.4(1)
Ce(2)/La(2)	1/2	0.096(1)	3/4	1.3(2)
I	0	0.985(1)	1/4	2.1(2)
Si	0.163(2)	0.460(3)	0.029(2)	2.1(8)
S(1)	0.144(1)	0.261(2)	0.137(2)	0.2(2)
S(2)	0.278(1)	0.557(3)	0.083(2)	0.2
S(3)	0.065(1)	0.653(2)	0.041(2)	0.2
S(4)	0.152(1)	0.396(3)	− 0.154(2)	0.2

2.3. Optical Measurements

Excitation and emission spectra were recorded with a Spex Fluorolog 212 spectrofluorometer. Excitation spectra were corrected for the variation of the incident flux as well as emission spectra for the transmission of the monochromator and the response of the photomultiplier. Reflectance spectra were obtained with the same equipment by simultaneously rotating the monochromators placed before and after the sample. Decay measurements were performed with a FL900 Edinburgh Instruments spectrometer which uses the time correlated photon counting technique. The excitation source was a hydrogen lamp delivering subnanosecond pulses.

3. RESULTS AND DISCUSSIONS

3.1. Structural Discussion

$Ce_3(SiS_4)_2X$ (X = Cl, Br) compounds. No particular discussion is to be made on the general structural features of these two compounds since they are both isostructural to $Ce_3(SiS_4)_2I$ (1, 2). It may be just recalled that these structures can be considered as constructed from a 3D $Ce_3(SiS_4)_2$ skeleton defining tunnels filled by Ce-bonded halogenides. A general view of the structure along the c axis is given in Fig. 1.

For each phase, the structural characteristics (bond distances and angles) are those expected. For instance, the

TABLE 3

Selected Bond Distances (Å) and Angles (°) in (a) $Ce_3(SiS_4)_2Cl$ and (b) $Ce_3(SiS_4)_2Br$ (ESD and Bond Multiplicity Between Brackets)

			(a)		
[Ce(1)S_8Cl] group:			[SiS_4] group:		
Ce(1)–S(1)	3.01(1)		Si–S(1)	2.02(2)	
Ce(1)–S(1)	3.21(1)		Si–S(2)	2.21(2)	
Ce(1)–S(2)	3.05(1)		Si–S(3)	2.21(2)	
Ce(1)–S(2)	3.09(1)		Si–S(4)	2.05(2)	
Ce(1)–S(2)	2.90(1)		Si–S	2.12	
Ce(1)–S(3)	2.88(1)		S(1)–Si–S(2)	107.5(9)	
Ce(1)–S(4)	2.97(1)		S(1)–Si–S(3)	111.7(9)	
Ce(1)–S(4)	2.99(1)		S(1)–Si–S(4)	115.1(9)	
Ce(1)–Cl	3.297(5)		S(2)–Si–S(3)	107.7(9)	
	3.01		S(2)–Si–S(4)	108.6(9)	
[Ce(2)S_8Cl] group:			S(3)–Si–S(4)	106.0(9)	
Ce(2)–S(1)	2.89(1)	(×2)	[$ClCe_3$] group:		
Ce(2)–S(3)	3.33(1)	(×2)	Cl–Ce(1)	3.304(6)	(×2)
Ce(2)–S(3)	3.35(1)	(×2)	Cl–Ce(2)	2.92(2)	
Ce(2)–S(4)	2.90(1)	(×2)	Cl–Ce	3.18	
Ce(2)–Cl	2.93(2)		Ce(1)–Cl–Ce(2)	106.3(3)	(×2)
Ce(1)–S	3.12		Ce(1)–Cl–Ce(1)	147.4(2)	
			(b)		
[Ce(1)S_8Br] group:			[SiS_4] group:		
Ce(1)–S(1)	3.02(1)		Si–S(1)	2.13(2)	
Ce(1)–S(1)	3.14(1)		Si–S(2)	2.15(2)	
Ce(1)–S(2)	3.03(1)		Si–S(3)	2.05(2)	
Ce(1)–S(2)	3.04(1)		Si–S(4)	2.05(2)	
Ce(1)–S(2)	2.91(1)		Si–S	2.09	
Ce(1)–S(3)	2.92(1)		S(1)–Si–S(2)	105.7(9)	
Ce(1)–S(4)	2.96(1)		S(1)–Si–S(3)	111.3(9)	
Ce(1)–S(4)	3.02(1)		S(1)–Si–S(4)	112.0(9)	
Ce(1)–Br	3.329(3)		S(2)–Si–S(3)	109.6(9)	
Ce(1)–S	3.00		S(2)–Si–S(4)	109.4(9)	
[Ce(2)S_8Br] group:			S(3)–Si–S(4)	108.8(9)	
Ce(2)–S(1)	2.90(1)	(×2)	[$BrCe_3$] group:		
Ce(2)–S(3)	3.30(1)	(×2)	Br–Ce(1)	3.329(3)	(×2)
Ce(2)–S(3)	3.29(1)	(×2)	Br–Ce(2)	3.125(8)	
Ce(2)–S(4)	2.91(1)	(×2)	Br–Ce	3.26	
Ce(2)–Br	3.125(8)		Ce(1)–Br–Ce(2)	104.6(2)	(×2)
Ce(2)–S	3.10		Ce(1)–Br–Ce(1)	150.7(1)	

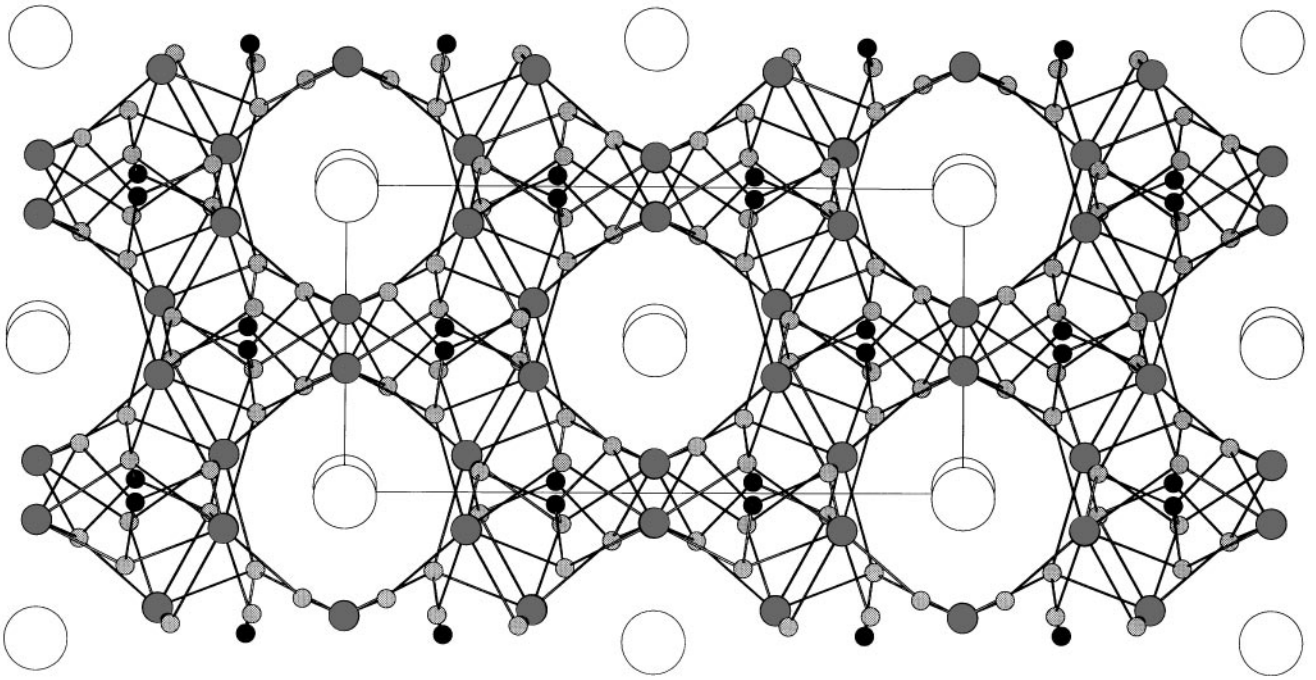

FIG. 1. View of $Ce_3(SiS_4)_2I$ down the *c* axis. Black atoms are Si, dark gray are Ce, light gray are S, and white are I. Each cerium atom is surrounded by eight S^{-II} and one I^- anions in (CeS_8I) polyhedra that can be regarded as (CeS_6) triangular prisms capped by two chalcogens and one halogen located in a plane perpendicular to the rectangular faces. I^- is coordinated by three cerium cations to form (ICe_3) isosceles triangles (see (2)).

Ce–S bond distances of the (CeS_8X) units range from 2.88(1) to 3.35(1) Å (average: 3.05 Å) in $Ce_3(SiS_4)_2Cl$ and from 2.90(1) to 3.30(1) Å (average: 3.03 Å) in $Ce_3(SiS_4)_2Br$, versus 2.904(2) to 3.285(2) Å (average: 3.037 Å) in $Ce_3(SiS_4)_2I$ (2). This agrees well with the sum of the ionic radii $rCe^{III} + rS^{-II} = 3.04$ Å (12). The Ce–S distances are thus quasi-independent of the nature of the halogenide. Otherwise, within the (XCe_3) groups, the Ce–*X* distances (Ce(2)–Cl = 2.93(2) Å, Ce(1)–Cl = 3.297(5) Å (*x*2) (average: 3.17 Å) (Table 3a), Ce(2)–Br = 3.125(8) Å, Ce(1)–Br = 3.329(3) Å (*x*2) (average: 3.26 Å) (Table 3b) and Ce(2)–I, 3.2954(9) Å, Ce(1)–I, 3.4324(4) Å (*x*2) (average: 3.39 Å) (2)), increase as expected from chlorine to iodine ($rCl^{-I} = 1.67$ Å, $rBr^{-I} = 1.82$ Å and $rI^{-I} = 2.06$ Å (12)). But whereas for the iodide the $\overline{Ce–X}$ distance compares satisfactorily well with the sum of the ionic radii of Ce^{III} and iodide ($rCe^{III} + rI^{-I} = 3.396$ Å) or with those observed for example in CeSI, i.e., from 3.301(1) to 3.4368(4) Å (13), these atomic distances depart somewhat from the expected ones for the chloride and bromide derivatives ($rCe^{III} + rX^{-I} = 3.006$ Å and 3.156 Å, respectively). Nevertheless, it has to be noticed that 3-coordinated halogenide ionic radii are not reported in the literature, and consequently, the theoretical distances tabulated in (12) may not fit the present halogenide coordination.

The Si–S bonds of the (SiS_4) groups range from 2.02(2) to 2.21(2) Å in $Ce_3(SiS_4)_2Cl$ and from 2.05(2) to 2.15(2) Å in $Ce_3(SiS_4)_2Br$. These values are close to those observed in $Ce_3(SiS_4)_2I$ (2.099(3) Å $< d_{Si–S} <$ 2.130(2) Å) and agree well with the sum of the ionic radii rSi^{IV}(C.N.4) + rS^{-II}(C.N.6) = 2.10 Å) (12).

Figure 2 presents the variation of the cubic root of the cell volume versus the ionic radius of the halogenide anion X^{-I} in the $Ce_3(SiS_4)_2X$ (X = Cl, Br, I) series. A linear relationship between these two parameters is observed. Nevertheless, it is worth mentioning that the cell expansion

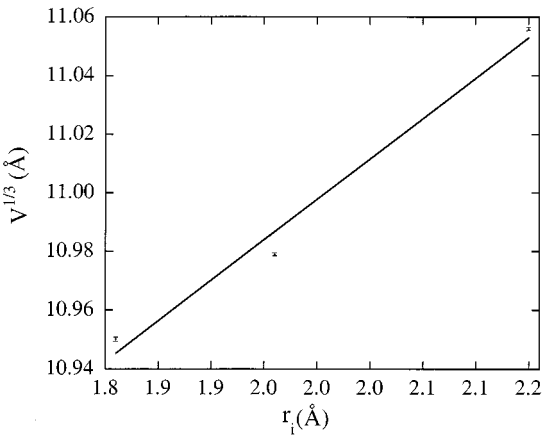

FIG. 2. Variation of the cubic root of the cell volume versus the ionic radius of the halogenide anion X^{-I} in the $Ce_3(SiS_4)_2X$ (X = Cl, Br, I) series.

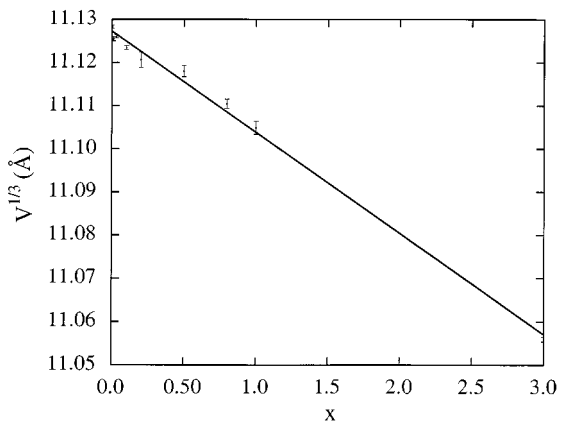

FIG. 3. Variation of the cubic root of the cell volume versus x in the $La_{3-x}Ce_x(SiS_4)_2I$ series.

is not isotropic; actually, the a and b parameters increase along the Cl, Br, I series, while an opposite trend is observed for the c parameter (Table 1). Moving from Cl^- to I^-, the halogenide induces increasing steric repulsions in the a and b directions, associated to in-plane Ce–X bonds, while weaker X^{-I}–X^{-I} electrostatic repulsion along the tunnels is the probable origin to the c parameter contraction.

$La_{3-x}Ce_x(SiS_4)_2I$ ($0 \le x \le 1$ and $x = 3$) solid solutions. As mentioned above, the X-ray pattern was assigned to a single phase. Nevertheless, we may note a slight increase of the peak full width at half maximum of the $La_{3-x}Ce_x(SiS_4)_2I$ ($0 < x \le 1$) compounds compared to those observed in $La_3(SiS_4)_2I$ and $Ce_3(SiS_4)_2I$. This suggests the possible occurrence of micro domains with different cationic compositions. Figure 3 shows the variation of the cubic root of the cell volume versus x. The observed linear decrease, from $La_3(SiS_4)_2I$ to $Ce_3(SiS_4)_2I$, confirms the long range random Ce/La distribution and is in agreement with the lanthanide contraction law ($r La^{III}$(C.N.9) = 1.216 Å and $r Ce^{III}$(C.N.9) = 1.196 Å) (12).

3.2. Optical Properties

3.2.1. Diffuse reflectance measurements. The reflectance spectra of $Ce_3(SiS_4)_2Cl$, $Ce_3(SiS_4)_2Br$, and $Ce_3(SiS_4)_2I$ show strong absorption properties up to about 410 nm (3.02 eV). For $La_3(SiS_4)_2I$, the absorption edge lies in the ultraviolet range, around 320 nm (3.87 eV), and has to be assigned to an electronic transition from predominantly anionic orbitals (valence band (vb)) to predominantly 5*d*–La orbitals (conduction band (cb)). This charge transfer transition is expected to be located at a similar energy threshold in Ce-containing parent phases. Moreover, since the energy of the vb → cb transition is expected to increase with decreasing size of the lanthanide ion as observed, for instance, in the $NaLnS_2$ series (14), the absorption between 320 and 420 nm (2.95 and 3.87 eV) in $Ce_3(SiS_4)_2Cl$, $Ce_3(SiS_4)_2Br$, and $Ce_3(SiS_4)_2I$ cannot be ascribed to vb → cb transitions but, without any ambiguity, to the $4f \rightarrow 5d$ intra-atomic cerium transition. This fact was already inferred from previous band structure calculations (1). Although the onset of this transition seems little influenced by the nature of the halogen, the absorption (α/S) data calculated from the reflectance, using the Kubelka–Munk function, lead to cerium 4*f*–5*d* band gaps of 2.77, 2.82, and 2.92 eV for $Ce_3(SiS_4)_2Cl$, $Ce_3(SiS_4)_2Br$, and $Ce_3(SiS_4)_2I$, respectively (Fig. 4). At longer wavelengths, the absorption is still elevated, indicating a high density of defects or small amounts of undetected impurities (15).

At this stage we may wonder what factors govern the 4*f*–5*d* energy gap. In order to unravel this point, let us indicate first extra absorption results obtained from $Ce_3(SiSe_4)_2I$ and $Ce_3(GeS_4)_2I$ (16). Both compounds are isostructural to $Ce_3(SiS_4)_2I$. The cerium iodothiosilicate and the cerium iodoselenosilicate show an absorption edge energy of 2.92 and 2.40 eV, respectively. This gap energy decrease of $\Delta Eg = 0.52$ eV is to be linked to higher covalency of the Ce–Se bond. As for $CePS_4$ and γ-Ce_2S_3, where the color shift from yellow ($\Delta_{4f-5d} = 2.49$ eV) to red ($\Delta_{4f-5d} = 1.89$ eV) originates from a decrease of the Ce–S bond ionicity character (17), the same phenomenon is observed between the thio and selenio compounds. Moreover, since the *s*, *p* energy levels of Ge lie higher in energy than those of Si, we expect a higher Ge–S bond ionicity. Consequently, through an inductive effect, the Ce–S interactions are expected to be more covalent (and the Ce–I one, more ionic) in $Ce_3(GeS_4)_2I$ than in $Ce_3(SiS_4)_2I$, inducing a reduction of the Δ_{4f-5d} gap for the former material. However, this gap reduction is less pronounced between the Si and Ge compounds ($\Delta Eg = 0.22$ eV) than between the sulfur and selenium derivatives ($\Delta Eg = 0.52$ eV). This is probably because of the second order effect of the main group element substitution.

Considering now the $Ce_3(SiS_4)_2X$ (X = Cl, Br, I) series, the enhancement of the Ce–X bond ionicity, from iodide to chloride, induces a higher Ce–S covalency (inductive effect), in good agreement with the reduction of the gap energy. The 0.15 eV energy shift from iodide to chloride suggests that the Ce–S bond is much less perturbed by the substitution of the halogenide than by a change of the main group element. This stems from the more polarizable character of sulfur compared with cerium. A slight modification of the electronic cloud around the chalcogen atoms, which mainly contributes to the occupied σ_{Ce-S} bonds, will induce more perturbations on the Ce–S bonds than a disturbance of the Ce electronic orbitals, whose *d* levels, in addition, essentially participate to unoccupied σ^*_{Ce-S} bonds. Hence, under an increase of the covalency of the Ce–S bond, a shift of the bottom of the conduction band to low energy is expected, in

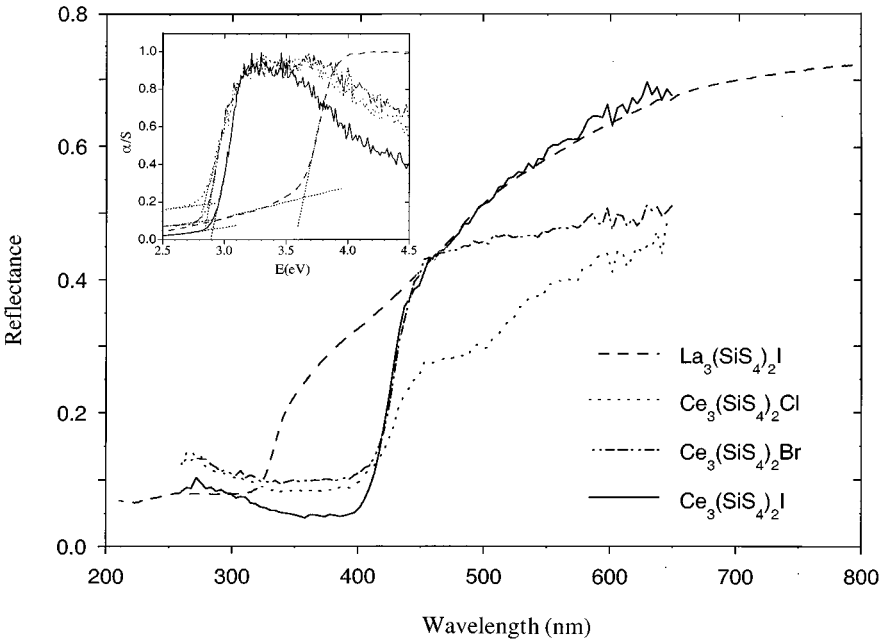

FIG. 4. Reflectance spectra of $La_3(SiS_4)_2I$, $Ce_3(SiS_4)_2Cl$, $Ce_3(SiS_4)_2Br$, and $Ce_3(SiS_4)_2I$ (in insert: Kubelka–Munk transformation and gap measurements).

relation to a higher dispersion of the Ce–d levels, while concomitant rising of the *f* levels is predicted, due to the larger screening effect of the nucleus by higher concentrated valence electrons around the cation (17, 18).

3.2.2. Luminescence properties. Excitation ($\lambda_{em} = 500$ nm) and emission ($\lambda_{exc} = 372$ nm) spectra at 300 K for the three cerium halothiosilicates are given in Figs. 5 and 6, respectively. From Fig. 5, the highest luminescence intensities are obtained for direct excitation of Ce^{3+} ions (from 350 and 400 nm) by $4f \rightarrow 5d$ transitions. From Fig. 6, the emission is found to occur in the form of a double characteristic broadband (bandwidth: 4040 cm^{-1} with I, 3800 cm^{-1} with Br, 4170 cm^{-1} with Cl) corresponding, in a prime analysis (see

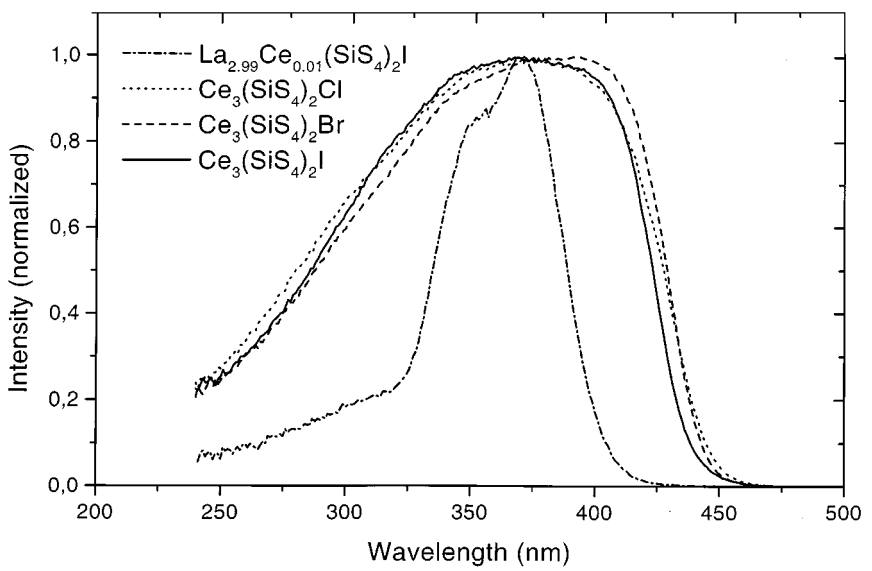

FIG. 5. Excitation spectra at 300 K ($\lambda_{em} = 500$ nm) of $La_{2.99}Ce_{0.01}(SiS_4)_2I$ and $Ce_3(SiS_4)_2X$ ($X =$ Cl, Br, I).

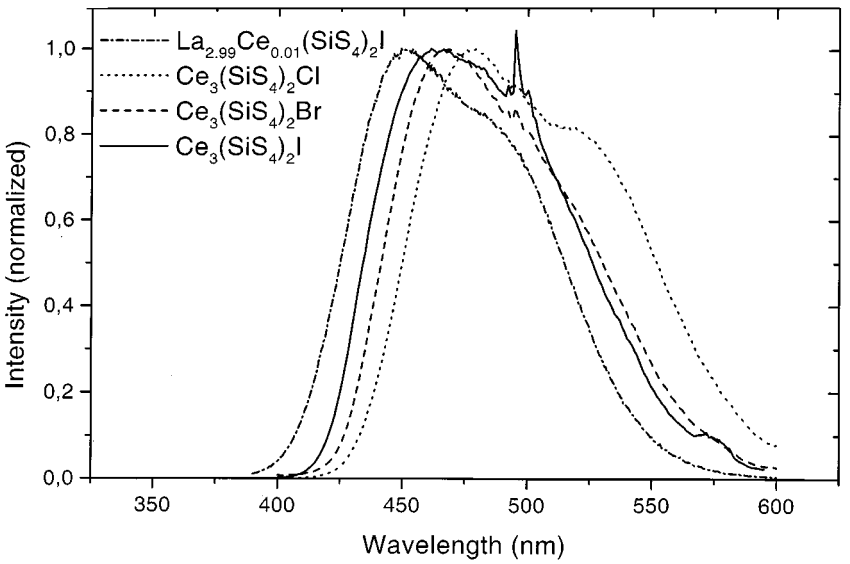

FIG. 6. Emission spectra ($\lambda_{exc} = 372$ nm) of $La_{2.99}Ce_{0.01}(SiS_4)_2I$ and $Ce_3(SiS_4)_2X$ (X = Cl, Br, I) at 300 K. The lines around 495 nm are due to traces of praseodymium in cerium starting materials.

below), to transitions from the lowest $5d$ state to the spin–orbit components, $^2F_{5/2}$ and $^2F_{7/2}$, of the $4f^1$ ground configuration. This band is displaced to shorter wavelengths with increasing size of the halogen (for excitation at 372 nm the maximum lies at 478, 468, and 465 nm, i.e., 2.59, 2.65, and 2.67 eV, respectively, for $Ce_3(SiS_4)_2Cl$, $Ce_3(SiS_4)_2Br$, and $Ce_3(SiS_4)_2I$). This shift is due to a slight change in the energy position of the Ce emitting level, as discussed in the previous paragraph, and to a variation of the Stokes shift. Formally, as a result of increased overlap between the Ce absorption and emission bands, the probability of energy migration to defects increases according to the sequence Cl < Br < I, as shown by the intensity of the 495-nm line, due to traces of praseodymium in the cerium sulfide used as starting material.

Figures 5 and 6 also give the excitation and emission spectra of cerium in the lanthanum iodothiosilicate for $x = 0.01$. The emission band is displaced by 11 nm to shorter wavelengths with respect to that of $Ce_3(SiS_4)_2I$. For higher Ce content ($x > 0.01$), this band shifts to longer wavelengths. To explain this emission threshold displacement, we may suggest either a contraction of the lattice causing a larger crystal field splitting of $5d$ levels, an emission band deformation (see Fig. 5, for $Ce_3(SiS_4)_2I$) at low wavelength due to a stronger absorption of Ce, or an electronic band width increase upon higher cerium concentration.

At low cerium concentration, the luminescence trichromatic coordinates of $La_{3-x}Ce_x(SiS_4)_2I$ are close to that of $SrGa_2S_4$:Ce ($x = 0.141$ and $y = 0.149$ for $x = 0.01$).

Otherwise, the $La_3(SiS_4)_2I$ matrix exhibits an intrinsic luminescence at low temperature. Excitation ($\lambda_{em} = 490$ nm) and emission ($\lambda_{exc} = 300$ nm) spectra at 6 K are given in Fig. 7. The intensity is maximum for excitation at a wavelength close to the absorption edge, i.e., 308 nm (4.025 eV). At 6 K, the emission consists of a band peaking at 490 nm with a bandwidth of 4000 cm^{-1} and a Stokes shift of 12,000 cm^{-1} (1.49 eV). Thermal quenching appears around 70 K, the emission being nearly completely extinguished at 300 K (Fig. 8). A luminescence for excitation near the absorption edge has been observed for other sulfides with closed-shells cations. This is the case for $CaGa_2S_4$ (19) and La_2S_3 (20). The luminescence of the iodothiosilicate may be of excitonic type as in the case of Ga_2O_3 (21). However, for La_2S_3, it was ascribed to transition of donor–acceptor type, the donor being assumed to be traps near the bottom of the conduction band (20). More investigations are needed to propose an interpretation for the emission of the iodothisilicate.

We know from the structure analysis that the cerium ions are distributed into two types of crystallographic sites (1,2). The luminescence of two kinds of Ce^{3+} ions may be observed by dilution with lanthanum ions and cooling. Figure 9 shows excitation and emission spectra at 6 K for the composition $La_{2.99}Ce_{0.01}(SiS_4)_2I$. The solid and the dashed lines correspond, respectively, to $\lambda_{em} = 500$ nm and $\lambda_{exc} = 370$ nm, and $\lambda_{em} = 410$ nm and $\lambda_{exc} = 345$ nm. Both excitation spectra consist of two well-defined bands located respectively at 370 and 330 nm for $\lambda_{em} = 500$ nm, and at 340 and 320 nm for $\lambda_{em} = 410$ nm. Each spectrum corresponds

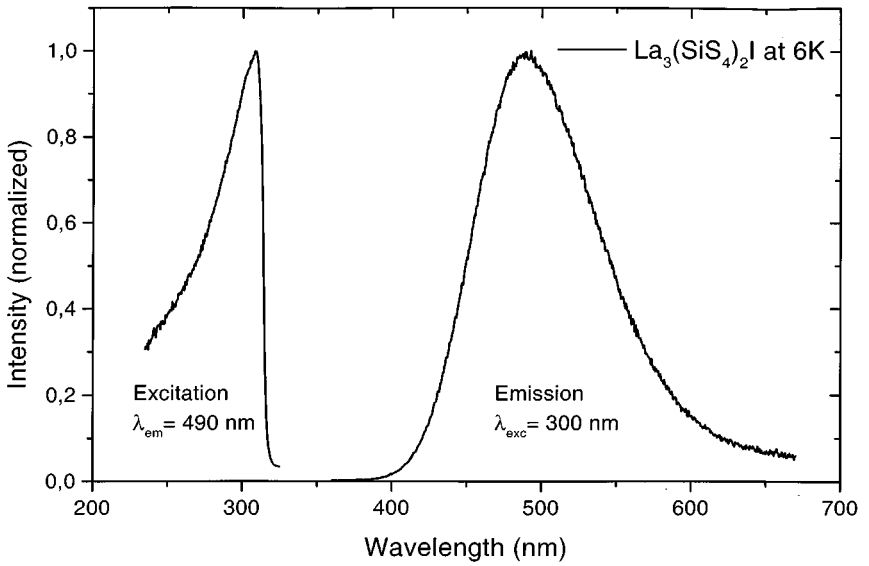

FIG. 7. (a) Excitation ($\lambda_{em} = 490$ nm) and (b) emission spectra ($\lambda_{exc} = 300$ nm) of $La_3(SiS_4)_2I$ at 6 K.

to the excitation of a cristallographically distinct cerium cation (see below). It is worth noticing that in both cases we may distinguish a very intense peak located at lower energy from a smaller one, which almost appears as a simple shoulder of the main peak for $\lambda_{em} = 410$ nm. In each case, the double band could be assigned to electronic transitions from the $^2F_{5/2}$ ground level to the different states coming from the crystal field and spin-orbit coupling effects on the $5d^1$ excited configuration. Let us notice that the observed band below 320 nm for $\lambda_{em} = 500$ nm is caused by the absorption in the host, but in fact, this emission wavelength corresponds to both cerium and exciton luminescences (see Fig. 7). There is very little overlap between the host emission and the cerium absorption, so for low dopant concentrations, low temperature excitation below 310 nm yields essentially the 490 nm band observed for $La_3(SiS_4)_2I$ in the absence of cerium.

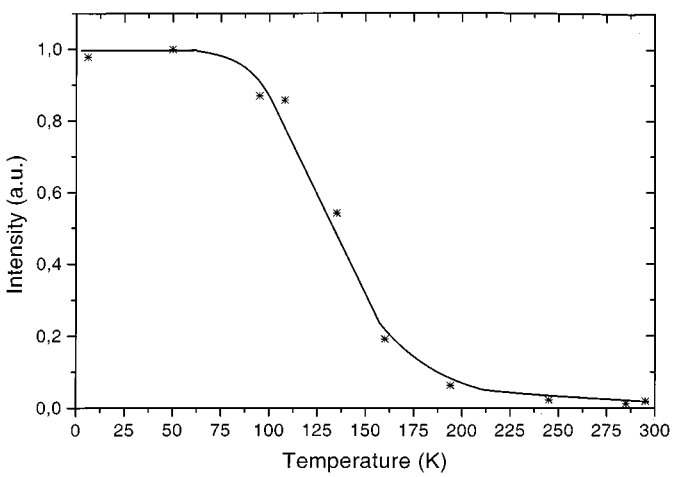

FIG. 8. Thermal variation of the emission intensity of $La_3(SiS_4)_2I$ ($\lambda_{exc} = 300$ nm).

Excitation in the 370 nm band selectively yields the emission spectrum of one type of cerium. The bands corresponding to the $5d \rightarrow {}^2F_{5/2}, {}^2F_{7/2}$ ($4f^1$) transitions are well separated and peak respectively at 446 and 491 nm. For excitation in the 345 nm band, a second emission peaking at 409 nm is predominant. Before normalization, its intensity is about twice lower than that of the longer wavelength emission (446 nm). Structurally, the Ce sites 1 and 2 are in the ratio 2/1. They show strong similarities so that comparable probabilities are expected for $4f \rightarrow 5d$ transitions. It can therefore be assumed that the 446 and 409 nm emissions correspond respectively to the sites Ce(1) and Ce(2). From the smaller size of sites 1 (1,2) a lowering of the position of the emitting $5d$ level is expected, thus decreasing the $5d \rightarrow 4f^1$ transition energies, in agreement with this assignment. The intensity of the 409 nm emission is reduced by energy transfer to the centers emitting at longer wavelengths with increasing temperature or Ce concentration. At 300 K, for small cerium concentrations, the shorter wavelength emission can still be distinguished for excitation at 345 nm. For $x = 1$ energy transfer to the Ce^{3+} ions emitting at longer wavelengths is total.

In the $La_{2.99}Ce_{0.01}(SiS_4)_2I$ compound, the Stokes shift of the two cerium emissions amounts to 4600 cm^{-1}, compared to 2000 cm^{-1} in $SrGa_2S_4$:Ce (22). While in the latter each sulfur atom is common to two (GaS_4) tetrahedra (23), in the halothiosilicates the (SiS_4) groups are isolated. The environ-

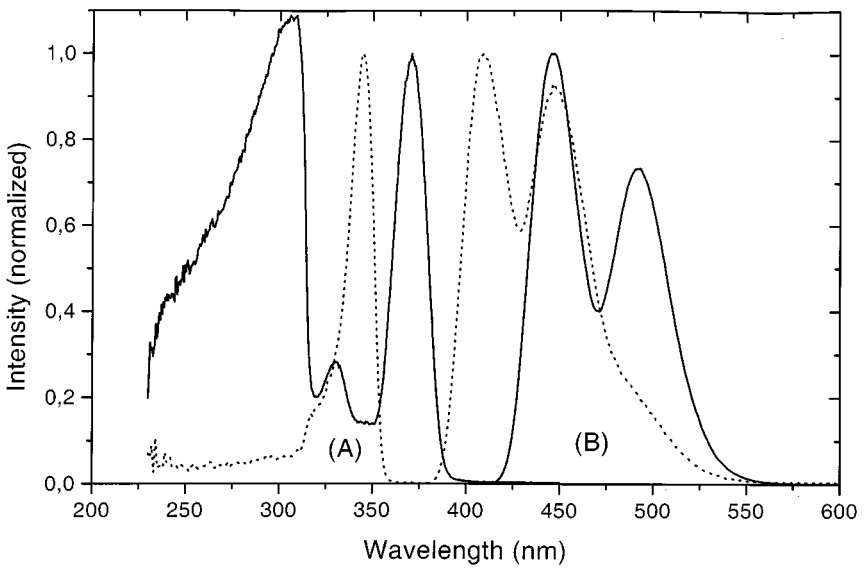

FIG. 9. Excitation (A) and emission (B) spectra for the two luminescences of Ce^{3+} in $La_{2.99}Ce_{0.01}(SiS_4)_2I$ at 6 K. (Solid line) A, $\lambda_{em} = 500$ nm, B, $\lambda_{exc} = 370$ nm. (Dotted line) A, $\lambda_{em} = 410$ nm; B, $\lambda_{exc} = 345$ nm. In the excitation spectrum for $\lambda_{em} = 500$ nm the band below 320 nm is caused by the emission of the host. The spectra are normalized at the maximum of the cerium transitions.

ment of Ce^{3+} ions being less rigid, a greater variation of the Ce–S bond is therefore expected when an electron is transferred from a 4*f* to a 5*d* orbital, resulting in a larger Stokes shift. Despite these relatively high values of the Stokes shift, the emission is not affected by thermal quenching at room temperature: for excitation at 372 nm the intensity of $La_{2.90}Ce_{0.10}(SiS_4)_2I$ decreases only by a few percent over the 6–300 K range as a result of the broadening of the absorption band. The low vibrational frequencies of bonds formed by sulfur and iodine atoms are favorable for a high stability of the emission (24, 25).

The cerium concentration dependence of the luminescence efficiency has been studied in the series $La_{3-x}Ce_x(SiS_4)_2I$. Figure 10 shows the variation of the internal quantum efficiency, i.e., the number of emitted to absorbed photons. The luminescence is affected by the presence of defects which absorb part of incident or emitted photons. This effect is particularly marked at low cerium concentrations. The large Stokes shift reduces the probability of energy migration from Ce^{3+} ions toward defects. For $Ce_3(SiS_4)_2I$ the quantum efficiency is reduced by only 25% with respect to the optimum composition.

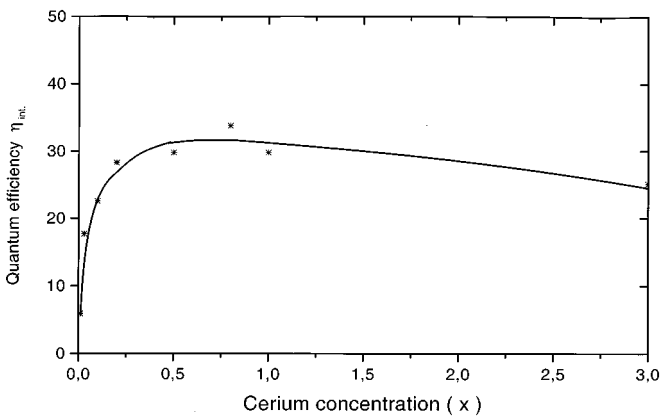

FIG. 10. Variation of the internal quantum efficiency for the series $La_{3-x}Ce_x(SiS_4)_2I$ ($\lambda_{exc} = 350$ nm).

After an initial fast component, up to $x = 0.8$, the luminescence decay curves of $La_{3-x}Ce_x(SiS_4)_2I$ show an exponential behavior over nearly two orders of magnitude. No variation of the decay time, $\tau = 18 \pm 1$ ns, has been detected, indicating that over this concentration range the probability of energy migration among Ce^{3+} is negligible. The small value of τ compared to those observed for Ce-doped oxides emitting in the visible (around 50 ns (26)) is probably the result of a high refractive index since the probability of radiative transition, $A_{rad.} = 1/\tau$, is proportional to $n(n^2 + 2)^2$ for electric dipole transitions.

4. CONCLUDING REMARKS

Lanthanum and cerium halothiosilicates are isostructural with the homologous halooxosilicates (27). In the latter family, the Ce^{III} emission lies in the ultraviolet, whereas, in the former, because of the covalency of the cerium–chalcogen bonding, the emission is displaced into the visible. In the lanthanum phase, the luminescence at 300 K is not affected by thermal quenching. Because of the weak rigidity of the lattice, the Stokes shift is high, so that concentration quenching is little pronounced. These two characteristics

are favorable for use of these compounds in electroluminescent devices. The color characteristic emission of Ce^{III} diluted in the lanthanum derivative are suitable for displays in the blue. Of course, the complexity of the formula may be an obstacle for the deposition of thin films. It may be noted that a drawback of $SrGa_2S_4$:Ce lies in its high crystallization temperature. In the new compounds the presence of halide could lower the latter below that of the thiogallate.

ACKNOWLEDGMENTS

The research has been made possible by a grant (CIFRE 260/96) from Rhodia and the "Association Nationale de la Recherche Technique." G. G., S. J., and R. B. acknowledge the sources of their financial support.

REFERENCES

1. G. Gauthier, S. Kawasaki, S. Jobic, P. Macaudière, R. Brec, and J. Rouxel, *J. Mater. Chem.* **8,** 179 (1997).
2. G. Gauthier, S. Kawasaki, S. Jobic, P. Macaudière, R. Brec, and J. Rouxel, *J. Alloys Comp.* **275–277,** 46 (1998). [Basis of the presentation given at ICFE3, 14–18 September, 1997]
3. H. Yamada, T. Kano, and M. Tanabe, *Mater. Res. Bull.* **13,** 101 (1978).
4. W. Lehmann and T. J. Isaacs, *J. Electrochem. Soc.* **125,** 445 (1978).
5. B. Es-Sakhi, C. Fouassier, and A. Moudden, *Ann. Chim. Sci. Mater.* **22,** 281 (1997).
6. G. Härkönen, M. Leppänen, E. Soininen, R. Törnqvist, and J. Viljanen, *J. Alloys. Comp.* **225,** 552 (1995).
7. S. S. Sun, R. T. Tuenge, J. Kane, and M. Ling, *J. Electrochem. Soc.* **141,** 2877 (1994).
8. P. Deniard, M. Evain, J. M. Barbet, and R. Brec, *Mater. Sci. Forum*, **363–382,** 79 (1991).
9. M. Evain, P. Deniard, A. Jouanneaux, and R. Brec, *J. Appl. Cryst.* **26,** 563 (1993).
10. J. Rodriguez-Carjaval, *Physica B* **192,** 55 (1993).
11. "International Tables for X-Ray Crystallography, Vol. III, Physical and Chemical Tables," (C. H. Macgillavry and G. D. Rieck, Eds., K. Lonsdale, Gen. Ed.), The Kynoch Press, Birmingham, England, 1968.
12. R. D. Shannon, *Acta Crystallogr.* **32,** 751 (1976).
13. H. P. Beck and C. Strobel, *Z. Anorg. Allg. Chem.* **535,** 229 (1986).
14. A. Garcia, R. Ibanez, and C. Fouassier, "Rare Earths Spectroscopy," p. 412. World Scientific, Singapore, 1985.
15. R. Pandey and S. Sivaraman, *J. Phys. Chem. Solids* **52,** 211 (1991).
16. R. Riccardi, private communication.
17. G. Gauthier, S. Jobic, F. Boucher, P. Macaudière, D. Huguenin, J. Rouxel, and R. Brec, *Chem. Mater.* **2341,** 10 (1998).
18. G. Gauthier, S. Jobic, R. Brec, and J. Rouxel, *Inorg. Chem.* **2332,** 37 (1998).
19. A. Garcia, Thèse de Doctorat d'Etat, Université Bordeaux I, 1984.
20. A. N. Georgobiani, M. V. Glushkov, E. S. Logozinskaya, Z. A. Pukhlii, I. M. Tiginyanu, and I. A. Shcherbakov, *Phys. State Solids* **76,** 311 (1983).
21. A. I. Kuznetsov, V. N. Abramov, and T. V. Uibo, *Opt. Spectrosc.* **58,** 368 (1985).
22. I. Ronot-Limousin, A. Garcia, C. Fouassier, C. Barthou, P. Benalloul, and J. Benoit, *J. Electrochem. Soc.* **144,** 687 (1997).
23. B. Eisenmann, M. Jakowski, W. Klee, and H. Schäfer, *Rev. Chim. Minér.* **20,** 255 (1983).
24. C. W. Struck and Fonger, *J. Lumin.* **10,** 1 (1975).
25. G. Blasse and N. Sabattini, *Mater. Chem. Phys.* **16,** 237 (1987).
26. G. Blasse and B.C. Grabmaier, "Luminescent Materials," Springer-Verlag, Berlin, 1994.
27. P. Gravereau, B. Es-sakhi, and C. Fouassier, *Acta Cryst. C* **44,** 1884 (1988).